Electronic Supplementary Information for

A structural study of the Ruddlesden-Popper phases $Sr_{3-x}Y_x(Fe_{1.25}Ni_{0.75})O_{7-\delta}$ with $x \leq 0.75$ by neutron powder diffraction and EXAFS/XANES spectroscopy.

Jekabs Grins, Dariusz Wardecki, Kjell Jansson, Stefan Carlson, Jordi J. Biendicho, Gunnar Svensson

PXRD data

Room temperature XRPD patterns were recorded with a PANalytical PRO MPD diffractometer with 1.5406 Å Cu $K_{\alpha 1}$ radiation, over a 2θ range of 15.0° to 140.0°, using variable slits with 20 mm irradiated length, a step size of 0.0131° and a total measuring time of 4.25 h, yielding maximum peak intensities of ~ 25000 counts. The samples contained small amounts of NiO, ~0.5wt%, and as-prepared samples also metallic Ni, ~ 0.2wt%, with the exception of phase pure x = 0.75 samples, which were included in the refinements. The recorded patterns are shown in Figures S1 and S2 with inserts showing the strongest NiO/Ni peaks.

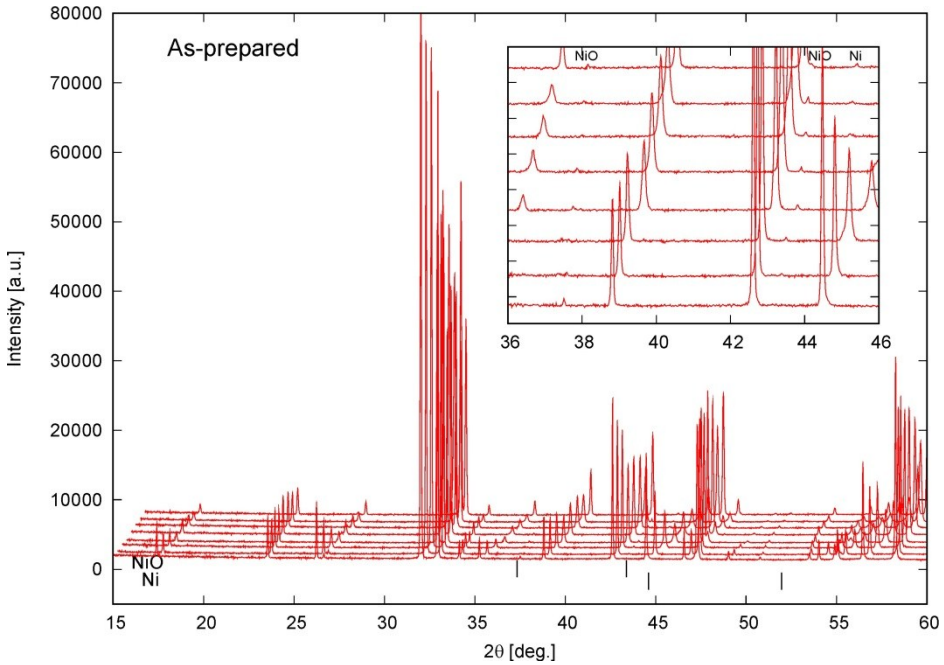

Figure S1. PXRD patterns for as-prepared samples, from back to front for x=0.0, 0.10, 0.20, 0.30 0.4, 0.50, 0.60 and 0.75. The data have been converted to fixed slit data. The insert shows the positions for the strongest peaks from NiO and Ni.

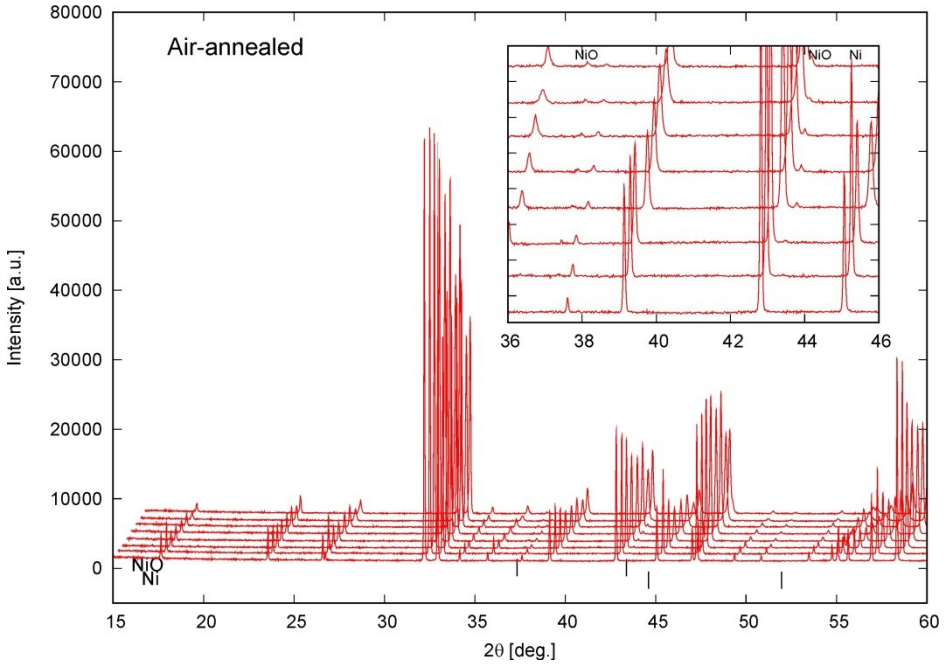

Figure S2. PXRD patterns for air-annealed samples, from back to front for *x*=0.0, 0.10, 0.20, 0.30 0.4, 0.50, 0.60 and 0.75. The data have been converted to fixed slit data. The insert shows the positions for the strongest peaks from NiO and Ni. No Ni metal could be detected for the air-annealed samples

Data from Rietveld refinements using NPD

Data were refined using the Topas software. A model was used containing up to 70 free parameters and including the crystal structure taken from L. Samain *et al.*, *J. Solid State Chem.*, 2015, **227**, 45. On the average data down to d = 0.3 Å were used and ~350 theoretical reflections. The peak shape and the background were modeled using a back-to-back function, described as a number 3 in the GSAS manual and Chebyshev polynomials, respectively. In order to improve the fit quality, the correction for the anisotropic peak broadening using 4th order symmetrized spherical harmonics was used (M. Järvinen, *J. Appl. Cryst.*, 1993, **26**, 525) as well as the Lobanov correction for the absorption (GSAS manual (2004)). For data from ISIS the three lower d value banks were used.

Table S1. Refinement data

	As-prepared					Air-annealed				
X		R_{exp} (%)	R_{wp} (%)	χ^2	R_I (%)		Rexp (%)	Rwp (%)	χ^2	R_I (%)
0.0	ORNL	1.5	2.8	3.7	3.4	ORNL	1.3	3.1	5.7	1.9
0.1	ORNL	1.3	2.0	2.4	0.8	ORNL	1.2	3.3	7.6	1.9

0.2	ISIS	2.8	3.7	1.8	1.5	ISIS	2.8	3.7	1.8	3.3
0.25	ORNL	1.2	2.2	3.5	5.4					
0.3	ISIS	1.1	3.1	7.9	1.7	ISIS	1.0	3.1	9.2	2.5
0.4	ORNL	1.1	3.3	9.2	2.2	ORNL	1.1	3.6	10.7	1.3
0.5	ISIS	1.3	3.4	7.4	3.0	ISIS	1.0	3.2	9.7	1.7
0.6	ORNL	1.1	3.6	10.7	1.4					
0.75	ORNL	1.5	4.4	8.4	6.6	ORNL	1.2	3.2	7.1	1.7

Table S2. Unit cell parameters

Unit cell parameters (Å)*						
	As-prepared			Air-annealed		
X	*a*	*c*	*V*	*a*	*c*	*V*
0.00	3.8394	20.3468	299.93	3.8433	20.1059	296.98
0.10	3.8520	20.2636	300.66	3.8435	20.0797	296.63
0.20	3.8643	20.1393	300.69	3.8423	20.0445	295.92
0.25	3.8685	20.0764	300.52	3.8418	20.0272	295.59
0.30	3.8714	20.0149	299.98	3.8412	20.0063	295.19
0.40	3.8754	19.9194	299.16	3.8395	19.9730	294.44
0.50	3.8748	19.8315	297.75	3.8389	19.9374	293.82
0.60	3.8713	19.7476	295.96	3.8392	19.9025	293.35
0.75	3.8661	19.6558	293.79	3.8389	19.8570	292.64

*From L. Samain et al., Journal of Solid State Chemistry 227, 45-54 (2015). From X-ray powder diffraction data. Estimated standard deviations are less than 0.001 Å for *a* and less than 0.0001 Å for *c*.

Table S3. Atomic coordinates for as-prepared samples.

Coordinates as-prepared samples				
X	z-A2	z-B	z-O1	z-O2
0.00	0.683352(41)	0.100431(28)	0.195017(46)	0.086833(40)
0.10	0.682922(52)	0.100215(37)	0.195008(65)	0.085383(69)
0.20	0.682263(40)	0.100057(29)	0.195200(47)	0.083449(40)
0.25	0.682177(46)	0.099885(31)	0.195435(56)	0.082385(48)
0.30	0.681756(33)	0.099522(24)	0.195373(40)	0.081580(31)
0.40	0.681453(41)	0.099195(27)	0.195342(50)	0.080114(44)
0.50	0.681091(38)	0.098528(26)	0.195346(44)	0.078630(38)
0.60	0.680830(50)	0.097770(40)	0.195150(60)	0.077280(50)
0.75	0.680490(30)	0.097020(30)	0.194930(30)	0.075610(30)

Table S4. Atomic coordinates for air-annealed samples.

Coordinates air-annealed samples				
X	z-A2	z-B	z-O1	z-O2
0.0	0.682016(37)	0.098988(25)	0.194062(46)	0.090945(39)
0.10	0.682181(42)	0.098528(27)	0.193982(49)	0.090546(44)
0.20	0.682070(30)	0.098113(23)	0.193695(37)	0.089450(32)
0.30	0.682121(32)	0.097769(22)	0.193689(35)	0.088231(30)

0.40	0.682058(41)	0.097413(28)	0.193532(44)	0.087123(43)
0.50	0.682008(33)	0.097161(24)	0.193572(31)	0.085496(31)
0.75	0.681831(40)	0.096792(28)	0.193722(43)	0.081569(46)

Table S5. Atomic displacement parameters for A and B atoms for as-prepared samples .

Displacement parameter for cations – as-prepared samples						
x	U11-A1	U33-A1	U11-A2	U33-A2	U11-B	U33-B
0.00	0.02387(45)	0.00779(46)	0.01572(29)	0.00692(33)	0.01221(20)	0.01335(35)
0.10	0.02261(61)	0.00946(71)	0.01478(40)	0.00830(48)	0.01098(28)	0.01123(47)
0.20	0.01447(36)	0.00745(53)	0.01254(28)	0.00806(36)	0.00826(17)	0.00941(36)
0.25	0.01362(33)	0.01002(50)	0.01305(27)	0.00981(37)	0.00796(17)	0.01230(37)
0.30	0.01000(27)	0.00864(43)	0.01137(22)	0.00922(33)	0.00756(14)	0.00883(30)
0.40	0.00939(30)	0.00883(46)	0.01178(25)	0.00967(38)	0.00556(16)	0.01150(36)
0.50	0.00785(25)	0.00736(40)	0.01168(23)	0.00835(34)	0.00381(13)	0.01113(30)
0.60	0.0065(3)	0.0053(5)	0.0114(3)	0.0101(5)	0.00301(13)	0.0111(4)
0.75	0.0055(2)	0.0062(3)	0.0125(2)	0.0071(3)	0.00396(9)	0.0083(2)

Table S6. Atomic displacement parameters for O atoms for as-prepared samples .

Displacement parameter for oxygen ions – as-prepared samples							
x	U11-O1	U33-O1	U11-O2	U33-O2	U11-O3	U22-O3	U33-O3
0.00	0.0355(23)	0.0074(19)	0.01964(35)	0.00812(46)	0.03420(65)	0.01822(53)	0.02806(65)
0.10	0.0514(52)	0.005	0.01869(46)	0.00696(59)	0.03207(85)	0.01181(61)	0.02979(92)
0.20	0.0319(55)	0.005	0.01635(31)	0.00436(43)	0.02714(50)	0.01037(39)	0.02775(64)
0.25	0.082(16)	0.026(14)	0.01669(27)	0.00732(44)	0.02413(45)	0.01140(37)	0.02878(59)
0.30	0.033(11)	0.005	0.01682(25)	0.00339(34)	0.02187(35)	0.00850(27)	0.02809(49)
0.40	-	-	0.01560(28)	0.00643(43)	0.01882(38)	0.00656(31)	0.02762(56)
0.50	-	-	0.01461(24)	0.00653(39)	0.01625(31)	0.00522(25)	0.02661(47)
0.60	-	-	0.0127(3)	0.0067(5)	0.0145(4)	0.0042(3)	0.0231(5)
0.75	-	-	0.0138(2)	0.0053(3)	0.0112(2)	0.00531(19)	0.0188(3)

Table S7. Atomic displacement parameters A and B atoms for air-annealed samples.

Displacement parameter for cations – air-annealed samples						
x	U11-A1	U33-A1	U11-A2	U33-A2	U11-B	U33-B
0.00	0.01166(29)	0.00351(41)	0.00603(19)	0.00491(29)	0.00229(13)	0.00849(27)
0.10	0.01351(32)	0.00351(42)	0.00611(19)	0.00538(29)	0.00264(12)	0.00724(27)
0.20	0.01570(30)	0.00228(39)	0.00592(17)	0.00449(27)	0.00267(10)	0.00596(23)
0.30	0.01688(75)	0.00302(74)	0.00639(72)	0.00485(69)	0.00312(69)	0.00312(69)
0.40	0.01835(32)	0.00600(41)	0.00756(18)	0.00672(29)	0.00347(10)	0.00729(22)
0.50	0.01889(79)	0.00387(77)	0.00679(77)	0.00487(74)	0.00343(73)	0.00607(81)
0.75	0.02242(37)	0.00542(41)	0.00843(19)	0.00657(31)	0.00324(10)	0.00606(22)

Table S8. Atomic displacement parameters for O atoms for air-annealed samples.

Displacement parameter for oxygen ions – air-annealed samples							
x	U11-O1	U33-O1	U11-O2	U33-O2	U11-O3	U22-O3	U33-O3
0.00	0.00869(64)	0.00132(85)	0.01015(25)	0.00547(37)	0.00700(25)	0.00656(24)	0.01839(41)
0.10	0.01098(73)	0.00215(90)	0.01087(26)	0.00482(39)	0.00909(28)	0.00703(25)	0.02168(46)

0.20	0.00970(67)	0.00000(80)	0.01090(25)	0.00358(34)	0.01224(26)	0.00701(22)	0.02535(42)
0.30	0.0128(10)	0.005*	0.01225(70)	0.00288(77)	0.01404(71)	0.00702(72)	0.03191(86)
0.40	0.01340(84)	0.005*	0.01285(26)	0.00557(40)	0.01469(29)	0.00606(24)	0.04026(58)
0.50	0.0192(12)	0.005*	0.01348(75)	0.00122(83)	0.01497(75)	0.00565(76)	0.04429(90)
0.75	0.0343(17)	0.0042(15)	0.01531(27)	0.00500(39)	0.01517(31)	0.00389(24)	0.05303(67)

* Fixed.

Table S9. Site occupancies for O atoms and O content per formula unit.

Site occupancy factors for O atoms and oxygen contents						
As-prepared				Air-annealed		
x	O1	O3	O content	O1	O3	O content
0.00	0.3348(48)	0.8131(28)	5.5872(74)	0.5521(55)	1*	6.5521(51)
0.10	0.2617(71)	0.8320(34)	5.5897(98)	0.5645(57)	1*	6.5645(57)
0.20	0.1238(40)	0.8710(25)	5.6078(64)	0.5461(33)	1*	6.5461(33)
0.25	0.1045(69)	0.9007(29)	5.7073(90)			
0.30	0.0503(32)	0.9170(20)	5.7183(51)	0.5395(44)	1*	6.5395(44)
0.40	0*	0.9393(27)	5.7572(54)	0.4949(46)	1*	6.4949(46)
0.50	0*	0.9622(26)	5.8488 (52)	0.4953(30)	1*	6.4953(30)
0.60	0*	1*	6*			
0.75	0*	1*	6*	0.4133(50)	1*	6.4133(50)

* Fixed.

Table S10. Interatomic distances for as-prepared samples.

Inter-atomic distances – as-prepared samples								
x	B-O1	B-O2	B-O3	A1-O1	A1-O3	A2-O2	A2-O2	A2-O3
0.00	2.0434(6)	1.925(1)	1.940(1)	2.7149(1)	2.609(1)	2.475(1)	2.725(1)	2.746(1)
0.10	2.0307(8)	1.921(1)	1.949(2)	2.7238(1)	2.589(1)	2.474(2)	2.735(2)	2.760(2)
0.20	2.0150(6)	1.916(1)	1.961(1)	2.7325(1)	2.561(1)	2.468(1)	2.745(1)	2.774(1)
0.25	2.0053(5)	1.918(1)	1.966(1)	2.7355(1)	2.545(1)	2.457(2)	2.748(1)	2.785(1)
0.30	1.9919(5)	1.9184(9)	1.969(1)	2.7375(1)	2.5324(6)	2.459(1)	2.751(1)	2.787(1)
0.40	1.9759(5)	1.915(1)	1.975(1)	2.7403(1)	2.5102(9)	2.454(1)	2.754(1)	2.798(1)
0.50	1.9540(5)	1.920(1)	1.977(1)	2.7399(1)	2.4870(8)	2.450(1)	2.754(1)	2.808(1)
0.60	1.9307(8)	1.923(1)	1.977(1)	2.7374(1)	2.465(1)	2.449(2)	2.752(2)	2.816(1)
0.75	1.9070(4)	1.9245(7)	1.9783(7)	2.7337(1)	2.4383(6)	2.4487(8)	2.7484(8)	2.8260(8)

Table S11. Interatomic distances for air-annealed samples

Inter-atomic distances – air-annealed samples								
x	B-O1	B-O2	B-O3	A1-O1	A1-O3	A2-O2	A2-O2	A2-O3
0.00	1.9902(5)	1.912(1)	1.9284(9)	2.7176(1)	2.6526(8)	2.492(1)	2.728(1)	2.654(1)
0.10	1.9784(5)	1.917(1)	1.928(1)	2.7178(1)	2.6455(9)	2.487(2)	2.728(1)	2.661(2)
0.20	1.9666(5)	1.9159(9)	1.9290(8)	2.7169(1)	2.6279(6)	2.490(1)	2.727(1)	2.672(1)
0.30	1.9562(4)	1.9192(8)	1.9301(7)	2.7162(1)	2.6087(6)	2.485(1)	2.726(1)	2.687(1)
0.40	1.9456(6)	1.920(1)	1.931(1)	2.7149(1)	2.5910(9)	2.485(1)	2.725(1)	2.698(1)
0.50	1.9371(5)	1.9221(8)	1.9334(8)	2.7144(1)	2.5670(6)	2.481(1)	2.724(1)	2.718(1)
0.75	1.9224(6)	1.925(1)	1.943(1)	2.7144(1)	2.5116(9)	2.472(8)	2.725(1)	2.766(8)

Table S12. Bond valence sums for as-prepared samples. Calculated from $BVS = \sum_i exp((r_0 - d)/0.37)$ with r_0 = 1.759 (Fe^{3+}) for B, 2.118 (Sr^{2+}) for A.

Bond valence sums – as-prepared samples						
x	B	A1	A2	O1	O2	O3
0.00	2.791	1.992	1.752	1.724	1.795	2.208
0.10	2.761	2.067	1.725	1.719	1.784	2.227
0.20	2.735	2.200	1.716	1.725	1.777	2.264
0.25	2.763	2.351	1.722	1.737	1.778	2.271
0.30	2.758	2.431	1.722	1.762	1.770	2.281
0.40	2.753	2.603	1.717	1.787	1.775	2.311
0.50	2.781	2.840	1.720	1.838	1.770	2.318
0.60	2.858	3.133	1.737	1.902	1.772	2.332
0.75	2.850	3.366	1.727	1.965	1.776	2.351

Table S13. Bond valence sums for air-annealed samples. Calculated from $BVS = \sum_i exp((r_0 - d)/0.37)$ with r_0 = 1.759 (Fe^{3+}) for B, 2.118 (Sr^{2+}) for A.

Bond valence sums – air-annealed samples						
x	B	A1	A2	O1	O2	O3
0.00	3.488	2.323	2.071	1.862	1.794	2.191
0.10	3.495	2.369	2.061	1.878	1.791	2.171
0.20	3.492	2.450	2.033	1.897	1.792	2.186
0.30	3.484	2.552	2.005	1.912	1.793	2.188
0.40	3.461	2.622	1.981	1.930	1.795	2.198
0.50	3.446	2.773	1.943	1.940	1.796	2.211
0.75	3.337	3.091	1.856	1.944	1.799	2.244

hkl dependent peak broadenings in powder diffraction data

We conclude that stacking faults is the probable cause of the *hkl* dependent peak broadenings. For the refinements from NPD data, they could be adequately modelled by spherical harmonics, as implemented in the TOPAS program. For higher-resolution synchrotron data it was necessary to also include an anisotropic asymmetry. The synchrotron data were recorded at the ID22 beam line (λ = 0.4009 Å) of the ESRF synchrotron radiation facility, Grenoble, France.

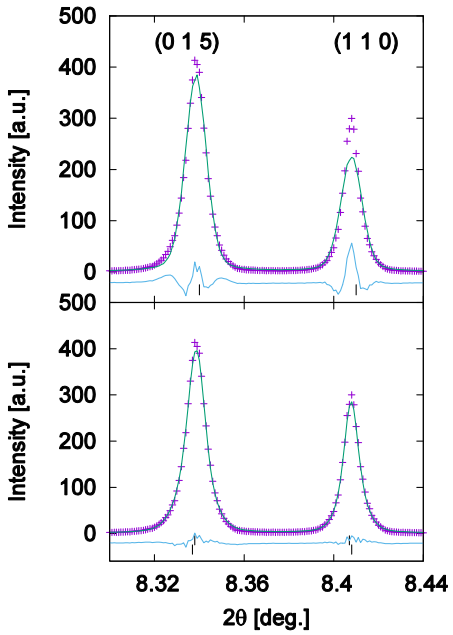

Figure S3. The 015 and 110 reflections for a refinement of the structure of as-prepared x = 0.75 from X-ray synchrotron data without (upper graph) and with (lower graph) including (i) an hkl-dependent strain broadening by spherical harmonics and (ii) an anisotropic asymmetry function.

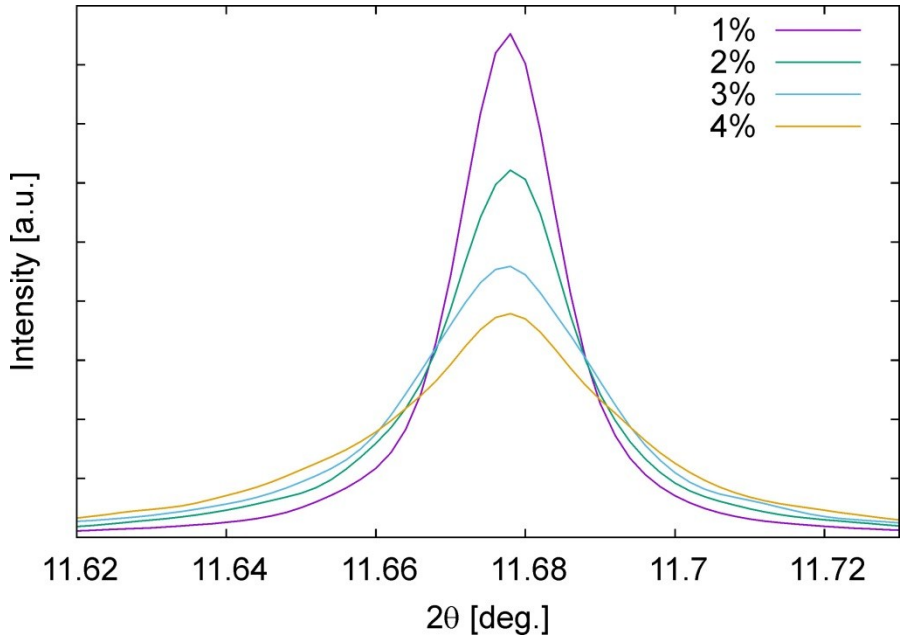

Figure S4. Simulated sample peak broadening from stacking faults by using the program Discus. The figure shows the peak (0 0 10) generated from 50000 layers along the *c*-axis for

1%, 2%, 3% and 4% of stacking faults, i.e., the perovskite *n*=2 double layer replaced by perovskite *n*=1 mono layer.

EXAFS

Analysis of EXAFS data provided information about (i) changes in Fe/Ni-O distances and thereby changes in oxidation states and coordination numbers of Fe/Ni and (ii) coordination numbers of Fe and Ni from peak intensities.

Air-annealed samples

The Rietveld refinements of the neutron diffraction data collected for the air annealed samples showed that the oxygen sites O2 and O3 are fully ocuppyed, whereas the site O1 is occupied to around 50%. Two possible oxygen coordinations of the B atoms are thus possible: square pyramids and ocatahedra. A schematic illustration of these two cases is given in Fig. SI5. Fe and Ni atoms can be coupled between the layers as shown; (I) Ni – Ni , (II) Fe – Ni, and (III) Fe – Fe. When an oxygen atom is present at the site O1, the focusing affect gives an extra intensity contribution in the EXAFS spectra at distances around 3.87 Å. This effect is more pronounced in the Ni spectra, which shows that the oxygen atoms at the O1 sites are coupled preferentially with Ni, rather then Fe.

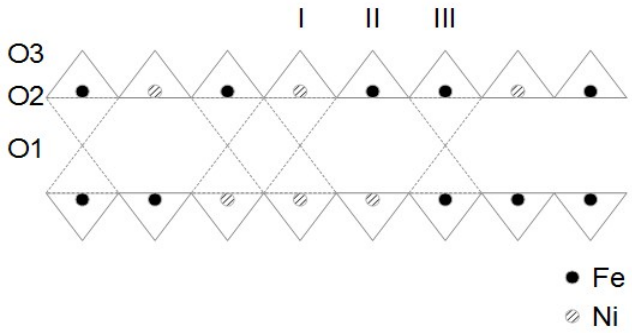

Figure S5. Schematic illustration of an perovskite double layer. The site O1, occupied to about 50 % by oxygen atoms, gives a contribution to the focusing effect between pairs Ni – Ni (I), Fe – Ni (II) or Fe – Fe (III) that causes intensity changes in the EXAFS spectra.

The fits of Fe – O distances for the first coordination shell suggest a small variation of Fe-O distances with *x*. No significant variation with *x* is observed for the Ni-O distance.

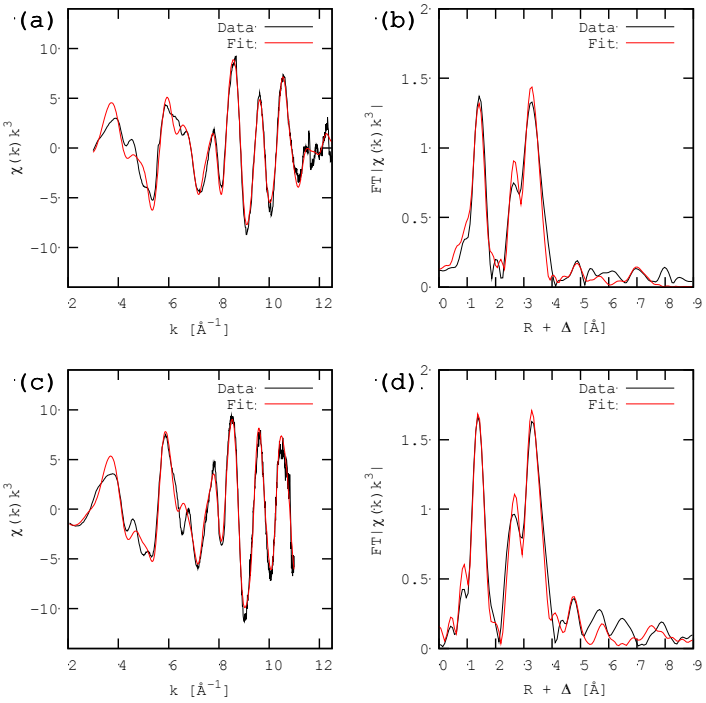

Figure S6. EXAFS data and fits for air-annealed samples x=0.10; (a,b) Fe and (c,d) Ni.

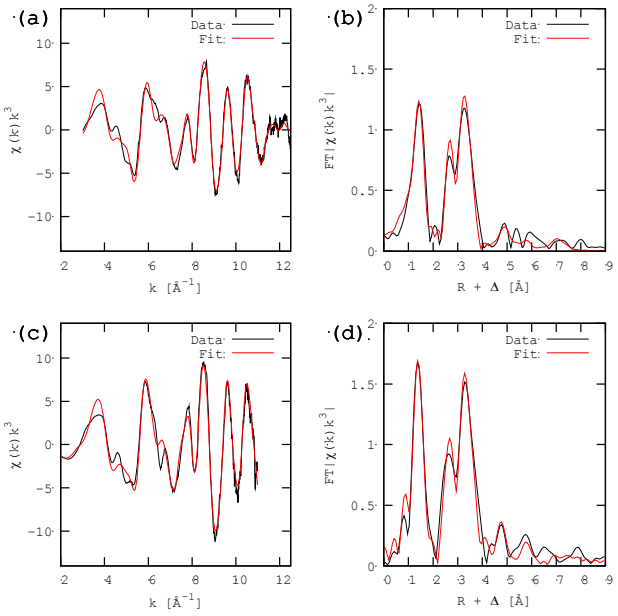

Figure S7. EXAFS data and fits for air-annealed samples x = 0.25; (a,b) Fe and (c,d) Ni.

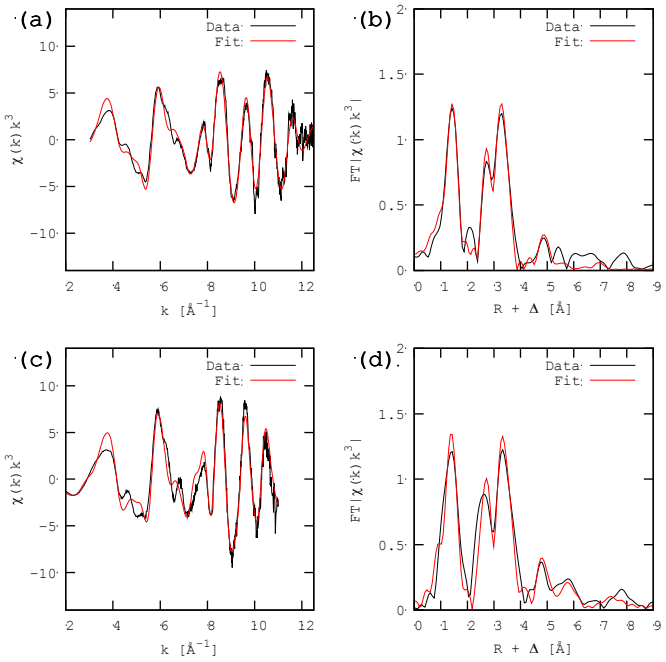

Figure S8. EXAFS data and fits for air-annealed samples *x*=0.50; (a,b) Fe and (c,d) Ni.

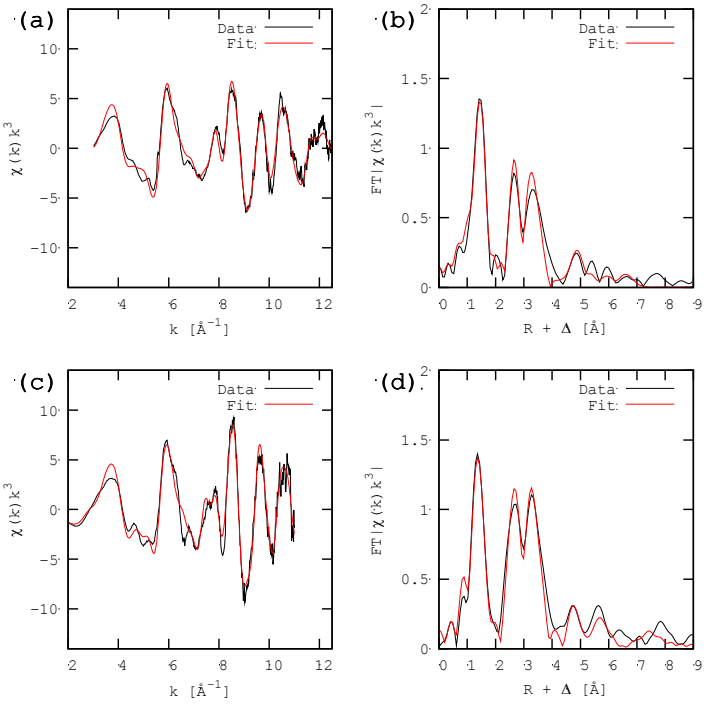

Figure S9. EXAFS data and fits for air-annealed samples *x*=0.75; (a,b) Fe and (c,d) Ni.

Table S14. Fitted parameters from the EXAFS data for Ni K-edge *x*=0.75 air-annealed.

Fitted parameters from the EXAFS data for Ni K-edge *x*=0.75 air-annealed					
Component	nleg	Degeneracy	Distance (Å)	σ^2 (Å^2)	Integral (%)
Ni – O	2	5.1(3)	1.941(3)	0.0058(4)	15.2
Ni – A1	2	4	3.203(3)	0.0046(2)	25.0
Ni – A2	2	4	3.43(2)	0.019(3)	1.8

Ni – B	2	5	3.868(7)	0.0040	19.0
Ni – B	3	4.8(1)	3.919(7)	0.0040	27.9
Ni – B	2	4	5.447(7)	0.0057(6)	4.8
Ni – A	2	16	6.37(1)	0.014(1)	3.5
Ni – A	7	2	8.16(1)	0.007(1)	2.7
Scale factor = 0.8, E_0 = -23.7(6) eV, weighted F-factor = 0.26, expected F-factor = 0.26					

Table S15. Fitted parameters from the EXAFS data for Ni K-edge *x*=0.50 air-annealed.

Fitted parameters from the EXAFS data for Ni K-edge *x*=0.50 air-annealed					
Component	nleg	Degeneracy	Distance (Å)	σ^2 (Å^2)	Integral (%)
Ni – O	2	5.5(3)	1.954(3)	0.0069(5)	14.0
Ni – A1	2	4	3.221(4)	0.0058(3)	19.7
Ni – A2	2	4	3.50(4)	0.021(5)	1.3
Ni – B	2	5	3.870(6)	0.0040	19.2
Ni – B	3	5.8(2)	3.920(6)	0.0040	33.7
Ni – B	2	4	5.471(7)	0.0057(6)	6.5
Ni – A	2	16	6.43(1)	0.014(1)	3.3
Ni – A	7	2	8.16(1)	0.008(1)	2.2
Scale factor = 0.8, E_0 = -21.7(6) eV, weighted F-factor = 0.30, expected F-factor = 0.25					

Table S16. Fitted parameters from the EXAFS data for Ni K-edge *x*=0.25 air-annealed.

Fitted parameters from the EXAFS data for Ni K-edge *x*=0.25 air-annealed					
Component	nleg	Degeneracy	Distance (Å)	σ^2 (Å^2)	Integral (%)
Ni – O	2	5.4(2)	1.940(2)	0.0043(3)	17.9
Ni – A1	2	4	3.219(4)	0.0050(3)	20.0
Ni – A2	2	4	3.48(1)	0.011(1)	5.4
Ni – B	2	5	3.854(5)	0.0040	17.1
Ni – B	3	5.8(2)	3.904(6)	0.0040	31.2
Ni – B	2	4	5.464(7)	0.0057(6)	4.3
Ni – A	2	16	6.41(1)	0.016(1)	2.1
Ni – A	7	2	8.13(1)	0.008(1)	2.0
Scale factor = 0.8, E_0 = -23.9(5) eV, weighted F-factor = 0.21, expected F-factor = 0.21					

Table S17. Fitted parameters from the EXAFS data for Ni K-edge *x*=0.10 air-annealed.

Fitted parameters from the EXAFS data for Ni K-edge *x*=0.10 air-annealed					
Component	nleg	Degeneracy	Distance (Å)	σ^2 (Å^2)	Integral (%)
Ni – O	2	5.6(2)	1.945(2)	0.0048(3)	16.4
Ni – A1	2	4	3.233(4)	0.0043(3)	21.1
Ni – A2	2	4	3.483(6)	0.008(1)	8.4
Ni – B	2	5	3.862(5)	0.0040	16.1
Ni – B	3	5.8(2)	3.913(6)	0.0040	29.4
Ni – B	2	4	5.475(7)	0.0054(6)	4.2
Ni – A	2	16	6.41(1)	0.018(1)	1.5
Ni – A	7	2	8.18(1)	0.006(1)	2.8

Scale factor = 0.8, E_0 = -23.9(5) eV, weighted F-factor = 0.21, expected F-factor = 0.21

Table S18. Fitted parameters from the EXAFS data for Fe K-edge *x*=0.75 air-annealed.

Fitted parameters from the EXAFS data for Fe K-edge *x*=0.75 air-annealed					
Component	nleg	Degeneracy	Distance (Å)	σ^2 (Å^2)	Integral (%)
Fe – O	2	4.4(1)	1.920(2)	0.0043(2)	19.4
Fe – A1	2	4	3.203(2)	0.0069(1)	19.3
Fe – A2	2	4	3.40(1)	0.018(2)	1.8
Fe – B	2	5	3.855(4)	0.0040	22.7
Fe – B	3	4.4(1)	3.904(4)	0.0040	29.2
Fe – B	2	4	5.459(5)	0.0062(4)	5.0
Fe – A	2	16	6.39(1)	0.014(1)	1.0
Fe – A	7	2	7.36(1)	0.012(1)	1.7
Scale factor = 0.8, E_0 = -24.5(5) eV, weighted F-factor = 0.26, expected F-factor = 0.34					

Table S19. Fitted parameters from the EXAFS data for Fe K-edge *x*=0.50 air-annealed.

Fitted parameters from the EXAFS data for Fe K-edge *x*=0.50 air-annealed					
Component	nleg	Degeneracy	Distance (Å)	σ^2 (Å^2)	Integral (%)
Fe – O	2	4.3(2)	1.912(2)	0.0045(3)	16.6
Fe – A1	2	4	3.237(3)	0.0067(2)	17.7
Fe – A2	2	4	3.498(3)	0.0086(4)	9.8
Fe – B	2	5	3.844(4)	0.0040	20.7
Fe – B	3	4.9(1)	3.894(4)	0.0040	29.9
Fe – B	2	4	5.481(6)	0.0065(5)	4.1
Fe – A	2	16	6.42(3)	0.025(4)	0.5
Fe – A	7	2	7.74(2)	0.015(3)	0.7
Scale factor = 0.8, E_0 = -23.7(5) eV, weighted F-factor = 0.26, expected F-factor = 0.29					

Table S20. Fitted parameters from the EXAFS data for Fe K-edge *x*=0.25 air-annealed.

Fitted parameters from the EXAFS data for Fe K-edge *x*=0.25 air-annealed					
Component	nleg	Degeneracy	Distance (Å)	σ^2 (Å^2)	Integral (%)
Fe – O	2	4.5(2)	1.905(2)	0.0051(2)	15.6
Fe – A1	2	4	3.217(2)	0.0065(1)	19.0
Fe – A2	2	4	3.485(4)	0.012(1)	4.9
Fe – B	2	5	3.852(3)	0.0040	20.8
Fe – B	3	5.5(1)	3.902(3)	0.0040	33.5
Fe – B	2	4	5.477(6)	0.0079(5)	3.2
Fe – A	2	16	6.46(1)	0.020(2)	1.0
Fe – A	7	2	7.78(1)	0.010(1)	1.9
Scale factor = 0.8, E_0 = -24.1(4) eV, weighted F-factor = 0.22, expected F-factor = 0.29					

Table S21. Fitted parameters from the EXAFS data for Fe K-edge *x*=0.10 air-annealed.

Fitted parameters from the EXAFS data for Fe K-edge *x*=0.10 air-annealed

Component	nleg	Degeneracy	Distance (Å)	σ^2 (Å^2)	Integral (%)
Fe – O	2	4.2(2)	1.892(2)	0.0040(2)	17.1
Fe – A1	2	4	3.205(3)	0.0069(2)	16.8
Fe – A2	2	4	3.502(5)	0.011(1)	5.6
Fe – B	2	5	3.838(3)	0.0040	19.9
Fe – B	3	6.0(1)	3.888(3)	0.0040	34.9
Fe – B	2	4	5.467(8)	0.0094(8)	2.2
Fe – A	2	16	6.42(2)	0.022(2)	0.7
Fe – A	7	2	7.75(1)	0.008(1)	2.7
Scale factor = 0.8, E_0 = -25.6(4) eV, weighted F-factor = 0.23, expected F-factor = 0.27					

As- prepared samples

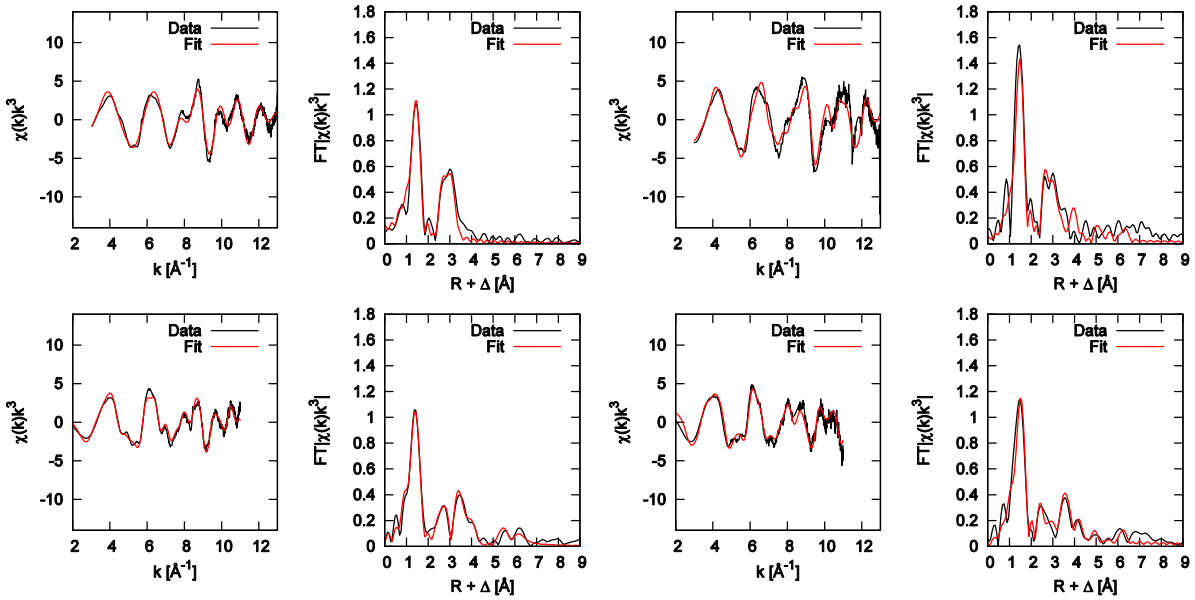

Figure S10 EXAFS data and fits for samples x=0.10 (left) and x=0.25 (right).

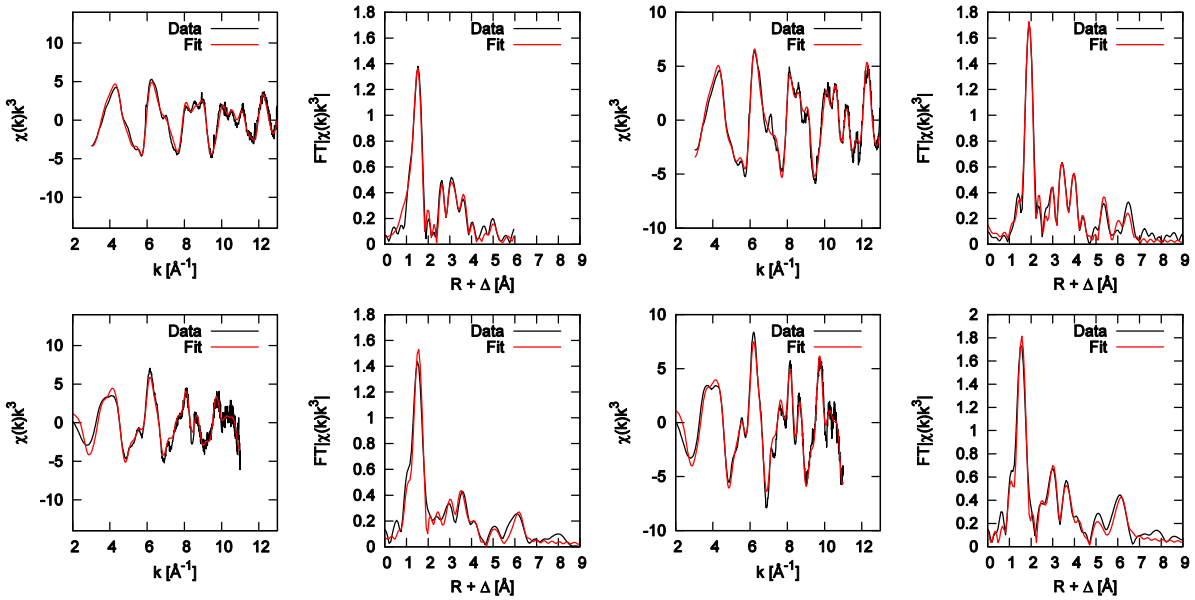

Figure S11. EXAFS data and fits for samples x=0.50 (left) and x=0.75 (right).

Table S22. Fitted parameters from the EXAFS data for Ni K-edge x = 0.75 N_2 prepared.

Fitted parameters from the EXAFS data for Ni K-edge x = 0.75 N_2 prepared					
Component	nleg	Degeneracy	Distance (Å)	σ^2 (Å^2)	Integral (%)
Ni – O	2	5	2.018(1)	0.0029(2)	29.0
Ni – A1	2	4	3.187(5)	0.0075(7)	18.4
Ni – A2	2	4	3.329(5)	0.0056(5)	23.2
Ni – B	2	5	3.996(4)	0.0075(3)	12.3
Ni – B	2	4	5.488(5)	0.0053(5)	6.4
Ni – A	2	16	6.429(4)	0.0084(3)	10.8
Scale factor = 0.7, E_0 = -7.0(3) eV, weighted F-factor = 0.22, expected F-factor = 0.30					

Table S23. Fitted parameters from the EXAFS data for Ni K-edge x = 0.50 N_2 prepared.

Fitted parameters from the EXAFS data for Ni K-edge x = 0.50 N_2 prepared					
Component	nleg	Degeneracy	Distance (Å)	σ^2 (Å^2)	Integral (%)
Ni – O	2	5	2.002(2)	0.0054(3)	35.2
Ni – A1	2	4	3.14(1)	0.013(1)	14.0
Ni – A2	2	4	3.30(1)	0.010(1)	19.4
Ni – B	2	5	3.992(5)	0.0094(4)	16.0
Ni – B	2	4	5.49(1)	0.010(1)	5.5
Ni – A	2	16	6.423(7)	0.0124(6)	9.9
Scale factor = 0.7, E_0 = -9.0(4) eV, weighted F-factor = 0.33, expected F-factor = 0.37					

Table S24. Fitted parameters from the EXAFS data for Ni K-edge x = 0.25 N_2 prepared.

Fitted parameters from the EXAFS data for Ni K-edge x = 0.25 N_2 prepared					
Component	nleg	Degeneracy	Distance (Å)	σ^2 (Å^2)	Integral (%)
Ni – O	2	5	1.968(3)	0.0056(4)	30.1
Ni – A1	2	4	3.141(7)	0.0087(7)	24.0
Ni – A2	2	4	3.31(1)	0.009(1)	20.8
Ni – B	2	5	3.991(5)	0.0074(5)	19.2
Ni – B	2	4	5.54(1)	0.016(1)	1.4
Ni – A	2	16	6.42(1)	0.016(1)	4.5
Scale factor = 0.7, E_0 = -10.9(5) eV, weighted F-factor = 0.41, expected F-factor = 0.47					

Table S25. Fitted parameters from the EXAFS data for Ni K-edge x = 0.10 N_2 prepared.

Fitted parameters from the EXAFS data for Ni K-edge x = 0.10 N_2 prepared					
Component	nleg	Degeneracy	Distance (Å)	σ^2 (Å^2)	Integral (%)
Ni – O	2	5	1.932(3)	0.0081(4)	37.4
Ni – A1	2	4	3.239(7)	0.0119(7)	23.1
Ni – A2	2	4	3.49(1)	0.014(1)	14.1
Ni – B	2	5	3.976(6)	0.0103(5)	21.6
Ni – B	2	4	5.34(6)	0.03(1)	0.6
Ni – A	2	16	6.40(1)	0.023(2)	3.1

Scale factor = 0.7, E_0 = -10.9(5) eV, weighted F-factor = 0.33, expected F-factor = 0.51

Table S26. Fitted parameters from the EXAFS data for Fe K-edge $x = 0.75$ N_2 prepared.

Fitted parameters from the EXAFS data for Fe K-edge $x = 0.75$ N_2 prepared					
Component	nleg	Degeneracy	Distance (Å)	σ^2 (Å^2)	Integral (%)
Fe – O	2	5	1.935(1)	0.0031(1)	25.8
Fe – A1	2	4	3.206(3)	0.0079(3)	14.7
Fe – A2	2	4	3.383(2)	0.0049(2)	25.8
Fe – B	2	5	3.949(5)	0.0052(6)	16.0
MS	3	1.5(3)	4.000(5)	0.0052(6)	6.8
Fe – B	2	4	5.490(5)	0.0062(6)	4.8
Fe – A	2	16	6.482(4)	0.0104(3)	6.2
Scale factor = 0.6, E_0 = -7.5(3) eV, weighted F-factor = 0.25, expected F-factor = 0.34					

Table S27. Fitted parameters from the EXAFS data for Fe K-edge $x = 0.50$ N_2 prepared.

Fitted parameters from the EXAFS data for Fe K-edge $x = 0.50$ N_2 prepared					
Component	nleg	Degeneracy	Distance (Å)	σ^2 (Å^2)	Integral (%)
Fe – O	2	4.0(1)	1.927(2)	0.0048(2)	24.2
Fe – A1	2	4	3.196(3)	0.0090(2)	18.6
Fe – A2	2	4	3.393(3)	0.0074(2)	23.2
Fe – B	2	5	3.95(1)	0.0071(8)	17.5
MS	3	2.2(4)	4.01(1)	0.0071(8)	11.6
Fe – B	2	4	5.54(1)	0.014(1)	1.6
Fe – A	2	16	6.52(1)	0.016(1)	3.3
Scale factor = 0.8, E_0 = -7.5(4) eV, weighted F-factor = 0.28, expected F-factor = 0.42					

Table S28. Fitted parameters from the EXAFS data for Fe K-edge $x = 0.25$ N_2 prepared.

Fitted parameters from the EXAFS data for Fe K-edge $x = 0.25$ N_2 prepared					
Component	nleg	Degeneracy	Distance (Å)	σ^2 (Å^2)	Integral (%)
Fe – O	2	4.0(1)	1.892(2)	0.0048(3)	29.8
Fe – A1	2	4	3.161(5)	0.0078(4)	24.7
Fe – A2	2	4	3.373(8)	0.0090(5)	16.7
Fe – B	2	5	3.91(4)	0.007(2)	16.5
MS	3	2.4(4)	3.97(4)	0.007(2)	11.7
Fe – B	2	4	5.4(1)	0.03(1)	0.1
Fe – A	2	16	6.9(1)	0.03(1)	0.5
Scale factor = 0.8, E_0 = -11(1) eV, weighted F-factor = 0.53, expected F-factor = 0.33					

Table S29. Fitted parameters from the EXAFS data for Fe K-edge $x = 0.10$ N_2 prepared.

Fitted parameters from the EXAFS data for Fe K-edge $x = 0.10$ N_2 prepared					
Component	nleg	Degeneracy	Distance (Å)	σ^2 (Å^2)	Integral (%)
Fe – O	2	5	1.898(2)	0.0048(1)	39.9
Fe – A1	2	4	3.167(2)	0.0080(2)	30.4

Fe – A2	2	4	3.348(3)	0.0091(3)	20.8
Fe – B	2	5	3.949(5)	0.0118(4)	9.0
Scale factor = 0.6, E_0 = -21.2(5) eV, weighted F-factor = 0.26, expected F-factor = 0.46					

XANES

All spectra were normalised to a height of one after the edge. The position of the main edge was taken as the energy at which the first derivative with respect to energy has a maximum. This occurred at a normalized height of about one. The position was calculated from using polynomial fits. The pre-edge was extracted by subtraction of the extrapolated left- and right-lying background All calculations were made using the computing package Maple 18.

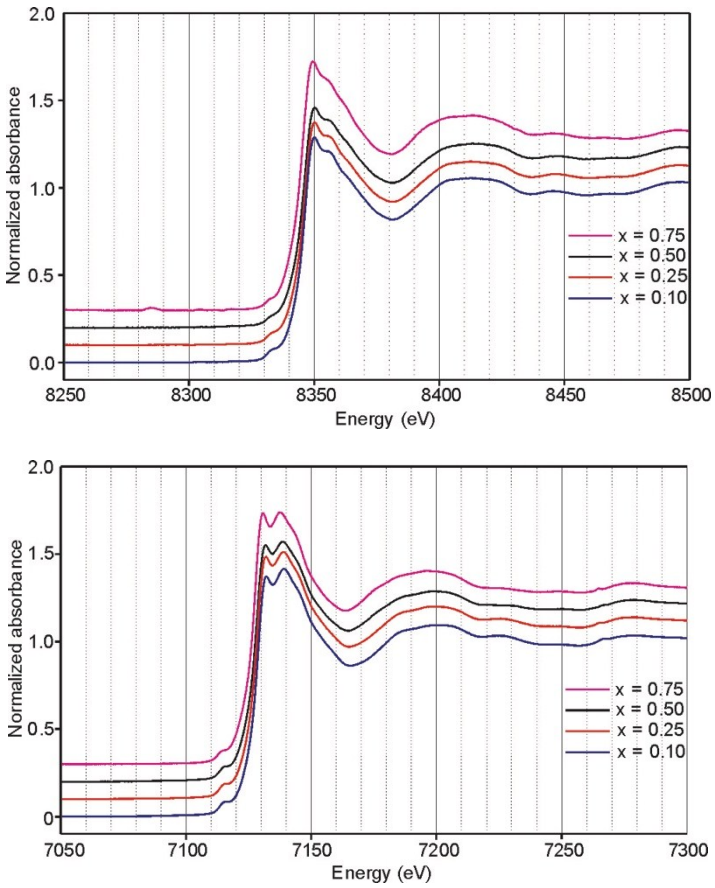

Figure S12. Ni and Fe XANES K-edge spectra for as-prepared samples.

Table S30. Data for Fe pre-edge.

Air	centroid position (eV)	height	area
0.10	7114.57	0.058	0.271
0.25	7114.56	0.056	0.262

0.50	7114.57	0.051	0.221
0.75	7114.42	0.048	0.198
N2			
0.10	7113.67	0.057	0.211
0.25	7113.52	0.049	0.214
0.50	7113.66	0.051	0.193
0.75	7113.58	0.054	0.223

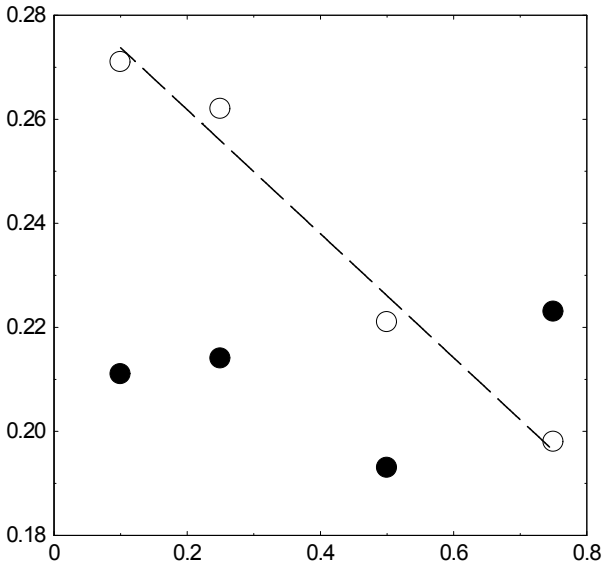

Figure S13. Fe pre-edge area intensity for as-prepared (filled circles) and air-annealed (open circles) samples.

Table S31. Data for Fe main edge.

Air	position (eV)	height at edge	maximum
0.10	7128.08	1.01	1.38
0.25	7127.84	0.83	1.38
0.50	7127.82	0.86	1.39
0.75	7127.50	0.92	1.44
N2			
0.10	7127.19	1.03	1.40
0.25	7126.78	1.03	1.41
0.50	7127.10	0.84	1.43
0.75	7127.20	1.06	1.52

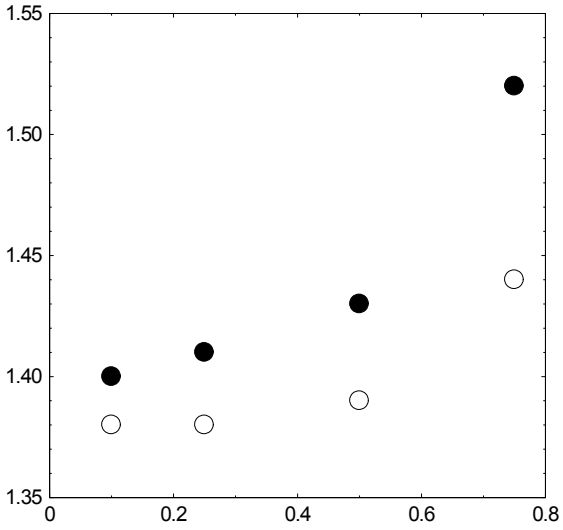

Figure S14. Fe main edge maximum intensity for as-prepared (filled circles) and air-annealed (open circles) samples.

Table S32. Data for Ni pre-edge.

air	Centroid position (eV)	area	height
0.00	8331.19	0.267	0.051
0.10	8331.79	0.186	0.039
0.20	8331.04	0.219	0.043
0.25	8331.68	0.162	0.035
0.30	8331.11	0.204	0.041
0.40	8330.84	0.185	0.038
0.50	8331.86	0.146	0.033
0.60	8331.41	0.160	0.032
0.75	8331.66	0.169	0.034
N2			
0.00*	8333.30	0.450	0.082
0.10*	8332.57	0.292	0.043
0.20*	8331.65	0.241	0.038
0.25*	8331.54	0.198	0.035
0.30*	8332.11	0.197	0.038
0.40	8330.26	0.175	0.039
0.50	8330.02	0.166	0.035
0.60	8329.38	0.175	0.022
0.75	8330.26	0.150	0.033

* Two peaks

Table S33. Data for Ni main edge.

air	position (eV)	height at edge	maximum
0.00	8347.54	1.04	1.45
0.10	8347.49	1.11	1.48

0.20	8347.28	1.01	1.45
0.25	8347.47	1.06	1.46
0.30	8347.42	1.02	1.45
0.40	8347.35	1.04	1.44
0.50	8347.26	1.03	1.43
0.60	8347.09	1.00	1.42
0.75	8347.12	1.06	1.42
N2			
0.00	8345.72	0.98	1.34
0.10	8345.62	0.98	1.39
0.25	8345.51	1.03	1.41
0.40	8345.80	1.07	1.47
0.50	8345.56	1.12	1.53
0.60	8345.64	1.09	1.53
0.75	8345.53	1.13	1.58

Pre-edge features

The pre-edge spectra were fitted using the fitting program fityk, version 0.9.8 (M. Wojdyr, J. Appl. Cryst., 43 (2010) 1126). Peaks were fitted using a pseudo-Voigt function, with a global shape but different half-widths in the case of several peaks.

Fe air-annealed samples.

For x=0.50 and x=0.75 the pre-edge consisted only of one peak with a half-width of ~4 eV, whereas for x=0.10 and x=0.25 the main peak had a small right wing, for x=0.10 at ~1.4 eV higher energy and relative intensity of ~10% and for x=0.25 at ~2.1 eV higher energy and a relative intensity of ~5%.

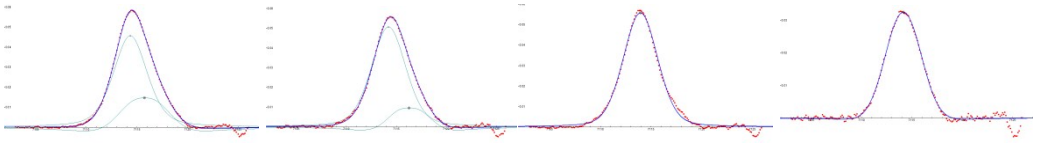

x=0.10 x=0.25 x=0.50 x=0.75

Figure S15. Fits of Fe pre-edge peaks for air-annealed samples.

Fe as-prepared samples.

For x=0.10 and x=0.25 the pre-edge consisted only of one peak with a half-width of ~4 eV, whereas for x=0.50 and x=0.75 the main peak had a small left wing, for x=0.50 at ~2.7 eV lower energy and relative intensity of ~14% and for x=0.25 at ~2.8 eV lower energy and a relative intensity of ~19%.

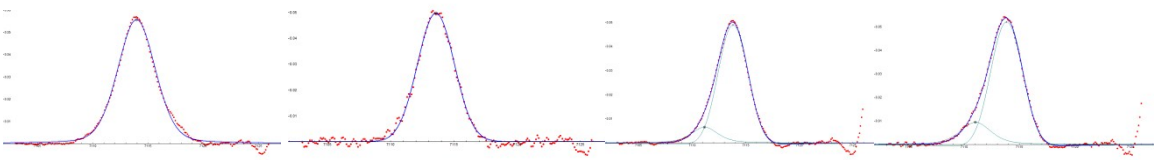

x=0.10 *x*=0.25 *x*=0.50 *x*=0.75

Figure S16. Fits of Fe pre-edge peaks for as-prepared samples.

Ni air-annealed samples.

For $0.0 \leq x \leq 0.50$ the pre-edge consisted only of one peak with a half-width of ~5 eV, whereas for x=0.60 and x=0.75 the main peak had a small left wing, for x=0.60 at ~3.2 eV lower energy and relative intensity of ~13% and for x=0.75 at ~2.9 eV lower energy and a relative intensity of ~24%.

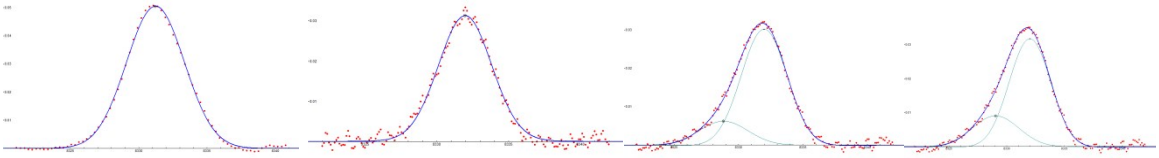

x=0.0 *x*=0.50 *x*=0.60 *x*=0.70

Figure S17. Fits of Ni pre-edge peaks for air-annealed samples.

Ni as-prepared samples.

For $0.0 \leq x \leq 0.4$ the pre-edge contains two peaks, separated by ~3.7 eV. The relative intensity of the higher energy peak decreases from ~63% for x=0.0 to ~10% for x=0.40. For $0.5 \leq x \leq 0.75$ the pre-edge contains also two peaks, with comparable relative intensities and separated by ~1.7 eV. The low-energy peak for $0.0 \leq x \leq 0.4$ is within error at the same energy as the high-energy peak for $0.5 \leq x \leq 0.75$.

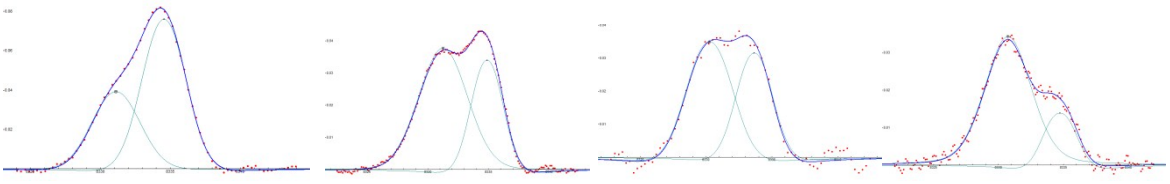

x=0.0 *x*=0.10 *x*=0.20 *x*=0.25

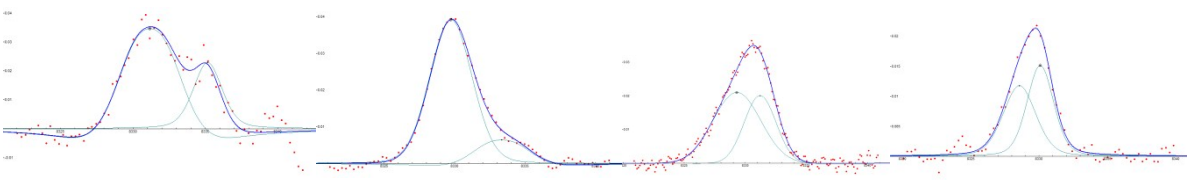

x=0.30 *x*=0.40 *x*=0.50 *x*=0.60

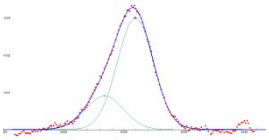

x=0.75

Figure S18. Fits of Ni pre-edge peaks for as-prepared samples.